Faraday Discussions
Cite this: *Faraday Discuss.*, 2014, **170**, 369

PAPER
View Article Online
View Journal | View Issue

Triboelectricity in insulating polymers: evidence for a mechanochemical mechanism

Lia Beraldo da Silveira Balestrin,[a] Douglas Del Duque,[a] Douglas Soares da Silva[a] and Fernando Galembeck[ab]

Received 4th December 2013, Accepted 17th February 2014
DOI: 10.1039/c3fd00118k

Transfer of reaction products formed on the surfaces of two mutually rubbed dielectric solids makes an important if not dominating contribution to triboelectricity. New evidence in support of this statement is presented in this report, based on analytical electron microscopy coupled to electrostatic potential mapping techniques. Mechanical action on contacting surface asperities transforms them into hot-spots for free-radical formation, followed by electron transfer producing cationic and anionic polymer fragments, according to their electronegativity. Polymer ions accumulate creating domains with excess charge because they are formed at fracture surfaces of pulled-out asperities. Another factor for charge segregation is the low polymer mixing entropy, following Flory and Huggins. The formation of fractal charge patterns that was previously described is thus the result of polymer fragment fractal scatter on both contacting surfaces. The present results contribute to the explanation of the centuries-old difficulties for understanding the "triboelectric series" and triboelectricity in general, as well as the dissipative nature of friction, and they may lead to better control of friction and its consequences.

1 Introduction

Triboelectricity formed on contacting surfaces has been known for centuries but the charge-formation mechanisms have never been well understood,[1–3] and they have been heavily debated in recent years.[4–7] A major issue is the identity of charge carriers and conflicting views have been presented by many authors, based on a great amount of experimental data. Disagreement on the nature of the charge carriers prevents scientists and engineers from developing a consensus on the

[a]*Institute of Chemistry, University of Campinas, Campinas, SP, Brazil 13083-970. E-mail: lia.balestrin@iqm.unicamp.br; douglas.duque@iqm.unicamp.br; dsoares@iqm.unicamp.br; fernagal@iqm.unicamp.br; Fax: +55 19 3521 2906; Tel: +55 19 3521 3014*
[b]*National Nanotechnology Laboratory, National Center for Energy and Materials Research, Campinas, SP, Brazil 13083-970. E-mail: fernando.galembeck@lnnano.cnpem.br; Fax: +55 19 3212 1004; Tel: +55 19 3518 3103*

mechanisms for charge build-up and dissipation. Since tribocharging takes place easily while handling small and large amounts of common commodities like sugar, wheat flour, polyethylene and coal, a practical consequence of the current state of knowledge on this topic is a long series of tragic events, explosions and fires, with losses of lives and property, recorded from many centuries ago to the present.[5,8–10]

1.1 Charge patterns on polymer surfaces

Since Kelvin force microscopy (KFM) and analogous techniques became available in the late nineties, they revealed[11] previously unexpected positive and negative charge domains patterned on the surfaces of any polymer sample that was examined in this and other groups.[12–15] Complex charge distribution patterns were also observed at the macroscopic scale by using scanning Kelvin electrodes,[16] suggesting a fractal character for the potential maps. Another unexpected finding was made by mapping the electrostatic potential on the surface of polytetrafluoroethylene (PTFE) rubbed with polyethylene (PE) foam and other polymer pairs: instead of the often-presumed uniform charge separation among the contacting solids that would make one object positive and the other negative, charged polymer surfaces display complex patterns and large electrostatic potential gradients are thus found along every insulating surface that has been handled or otherwise exposed to the environment. On the other hand, spatial control of surface charging is opening the way to a new kind of electrostatic lithography.[17] Thus, the widespread belief on the formation of separate positive and negative surfaces when two polymer (and other dielectric) surfaces are sheared, rubbed or rolled against each other[18] is not correct. Recognizing this now allows us to understand why there has never been full agreement on setting up a triboelectric series and also why the related quantitative data are not usually presented or available.[19]

1.2 Charge carriers on polymer surfaces

The identification of separate macroscopic domains with opposite charges in the same surface allowed the identification of the charged species formed on PTFE rubbed with PE by using a range of analytical techniques (infrared microspectrophotometry and Raman confocal microscopy, electron-energy loss spectroscopy and controlled pyrolysis), showing that the positive charge derives from the PE hydrocarbon chains while the negative charge is associated with PTFE fluorocarbon fragments, as expected considering the relative positions of PE and PTFE in most triboelectric series. In recent work from this group, charge pattern formation was interpreted as the result of polymer chain breakdown forming free radicals and ions, followed by electron transfer according to the electronegativity of each of these high-energy species formed.[17] Another puzzling observation is charge separation forming adjacent surface electrets instead of the more intuitive ion-pair formation. However, the general tendency of polymers to segregate into immiscible domains instead of mixing, albeit to a limited extent, as most other substances do easily explains charge separation at the micro- and macroscales, when charges are associated with polymer fragments. We recall that the main limitation to polymer miscibility is the positive enthalpy of mixing coupled to the very small mixing entropy of macromolecular substances, as first explained by Flory[20] and Huggins.[21]

1.3 Mechanochemical reactions, triboelectricity and friction coefficients

Mechanochemical reactions triggered by friction are thus the starting point for understanding a number of complex, challenging problems in tribology, from triboelectricity to the dependence of friction coefficients on surface modification during friction.[22]

Finding that tribocharging is the result of mechanochemical polymer reactions allows us to understand the appearance of surface charge on two rubbed samples of the same material (polisiloxane) that was presented by Baytekin *et al.*, as the result of fluctuations of chemical and micromechanical properties in the solids.[14]

One important question that was not yet fully addressed is this: is charge conserved during polymer (and other dielectrics) contact or tribocharging; this means, is the total amount of charge found in the two involved solids equal to the initial charge? Charge conservation is consistent with models and hypotheses based on charge transfer from one solid to another, either ions or electrons, due to any of the various properties of the two solids involved that have been considered by various authors. These properties are, for instance: correlations with the dielectric constant, the basic and acidic nature of the materials, the polymer work function and the surface chemistry determined by measuring the residence time of probe molecules using inverse gas chromatography.[2] On the other hand, recent work from this group[23,24] showed that the atmosphere is a charge reservoir. Water ions were identified as the carriers transferring charge between the solid (and also liquid) surfaces and the atmosphere. Thus, they participate in tribocharge formation: net positive or negative charge on a polymer surface includes contributions from polymer ions formed mechanochemically and distributed on the two involved surfaces added to excess H^+ and OH^- ions adsorbed from the atmosphere together with water vapour.

The observation of macro- and nano-scale charge patterns is consistent with the fractal nature of charge distribution that was shown experimentally earlier.[22] These findings led to additional work showing the effect of tribocharge formation on the rolling and sliding friction coefficients and also to direct experimental evidence for the modification of surface morphology at the nano-scale concurrent with friction.[22]

The identification of the role of free-radicals in tribocharge formation in polymers has already had an important outcome with a great potential for practical application: the demonstration that α-tocopherol, the important vitamin E that is effective as a free-radical suppressor in living bodies, contributes to diminish harmful charge from semiconductor encapsulants.[25]

The effect of mass transfer on the friction properties of solids has been well established in the literature for many years.[26,27] Excellent examples of direct microscopic examination of the sheared, rolled or rubbed surfaces are now found in the literature.[28,29,30] Beyond this, thin films of PTFE produced by friction deposition were studied using grazing incidence X-ray diffraction as the principal tool, showing structural surprises.[31] However, the association between all these phenomena and electrostatic charging of solid surfaces is very recent.[17]

This work presents new results on polymer fragment transfer between rubbed surfaces and their association with tribocharging, using electron microscopy and microanalysis tools that were not previously used in this context and provided

previously unavailable information. A main result is the demonstration of a broad size distribution for the transferred fragments that further helps to understand the observed separation of large positive and negative charge domains.

2 Experimental

2.1 Materials

The following polymer materials were used: LDPE foam disks (∅ = 15.0 mm, 3.3 mm thick, Nalgene 6283-1850), technical grade HDPE stubs (∅ = 13.5 mm, 11.2 mm height), PTFE stubs (∅ = 13.5 mm, 11.2 mm height), HDPE films (1 mm thick), PTFE films (1 mm thick), PTFE spheres (precision, ∅ = 3.969 mm), polystyrene Petri dish (∅ = 64 mm, 1.0 mm thick body). Pellets of nylon 6, nylon 6,9, nylon 12, polyacetal and HDPE (*ca.* 2 mm × 2 mm × 2 mm) were from Aldrich. Ethanol (99.5%, Synth) was used for sample cleaning. Materials identity was verified by IR spectra or DSC.

2.2 Methods

2.2.1 Sample cleaning and drying. Polymer films and stubs were immersed in ethanol for 10 min and dried in air for 2 h to minimize pre-existing static charge.

2.2.2 Tribocharging. Two methods for tribocharging were used:

2.2.2.1 Stub spinning. Square polymer films or disks (5 × 5 cm^2) were placed on an aluminum holder mounted on a table-top balance (AM 5500 Automarte, 10 mg resolution) and were rubbed with an LDPE foam disk or polymer stubs fitted on the chuck of a drilling tool spun at 5000 rpm for 3 s. Force applied on the sample was measured using the balance, to produce 12 kPa when using the stubs and 1.5 kPa using PE foam. Fig. 1 shows a picture and schematic description of the experiment.

2.2.2.2 Shaking. The cover of a Petri dish was mounted on top of an aluminum plate that was laid on the horizontal table of a reciprocating shaker. Two grams of pellets were spread on top of the dish and the setup was shaken for 40 min, with a 2.5 Hz reciprocating frequency and 20 mm amplitude. The HDPE film was shaken with 3 g PTFE spheres, for 120 min, 5 Hz and 10 mm amplitude.

2.2.3 Potential mapping. Charge patterns on the polymer surface were determined using a Kelvin electrode mounted on a computer-controlled moving

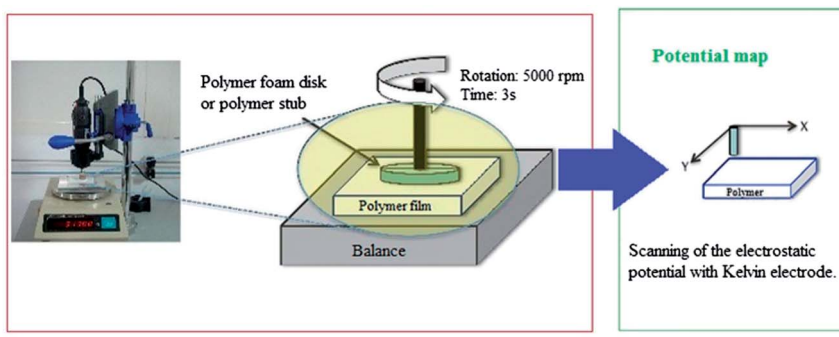

Fig. 1 Experimental sketch of a tribocharging experiment.

arm scanning the x–y plane (Optron) and connected to a voltmeter (model 347, Trek, 25 mm^2 area).

2.2.4 SEM. The samples were placed on a metallic sample holder and coated with a thin gold or carbon layer, using a MCS 010 Sputter (Bal-Tec). Morphological and chemical composition analysis of tribocharged samples were done on a JEOL JSM-6360 LV scanning electron microscope. The acceleration voltage in the reported experiments was 15 kV. Energy dispersive X-ray analysis (EDX) was done in the same microscope with a Noran System Six microanalysis system.

2.2.5 Infrared spectra. ATR/IR spectra were acquired with an IlluminatIR II instrument (Smiths) coupled to an Olympus BX51 microscopic using a ZnSe window in the spectral range between 650 and 4000 cm^{-1}, with 64 scans and 4 cm^{-1} resolution.

3 Results

The results reported here give new evidence for mass transfer between rubbed polymer surfaces producing wear and showing that mass transfer is always concurrent with charge deposition and patterning at the polymer surfaces. On the other hand, transfer is possible thanks to mechanochemical polymer chain scission that takes place either by rupturing separate chains or in a concerted way, when many chains are disconnected at once, allowing a polymer particle to be pulled out of one rubbing surface, landing on another spot on either surface.

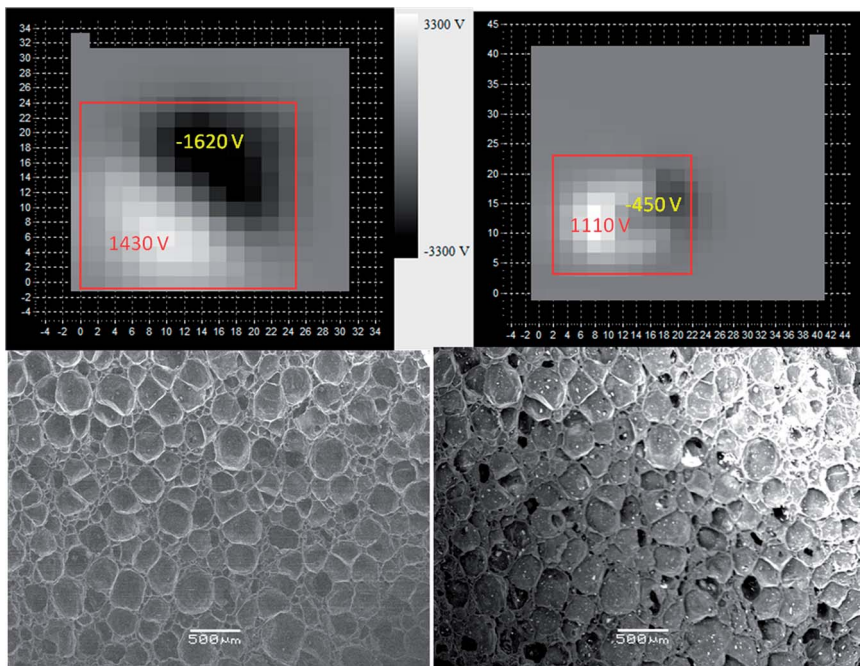

Fig. 2 (Top) Electrostatic potential maps of PTFE film (left) sheared with LDPE foam slabs (right). The average potential of the positive and negative region of each material is printed in the respective area. (Bottom left) SEI micrograph of a negative area of sheared LDPE foam. (Bottom right) BEI micrograph of the same area.

Scanning electron micrographs of a negative area of LDPE foam surface sheared with PTFE are shown in Fig. 2. The SEI micrographs show the expected morphology but BEI reveals that this surface contains many brighter or darker domains contrasting with the dominating gray tone. Brighter domains in BEI composition images are areas with a higher average atom number as compared to others. In a sample containing only hydrocarbon and fluorocarbon, the brighter regions are fluorine-rich.

EDX analysis shows the presence of 2.4 atom% fluorine in one of the bright spots while other areas contained also Ca and Mg, released by the foamed LDPE. It is important to keep in mind that the analytical information conveyed by BEI and EDX do not necessarily match, because the sampling depth is different in the two cases: usually, backscattered electrons sample a thinner layer more adjacent to the surface than EDX.

Elemental distribution maps of C, F and O for another related area are in Fig. 3, showing the superposition of these three elements on the LDPE surface and evidencing that oxygenated species were also formed during tribocharging.

Similar examination was done in an electrically positive spot on the foam surface. Again, contrast assigned to changing chemical composition was observed but point analysis did not detect F in any tested spot while the dots in the F map are barely above noise. Thus, fluorocarbon transfer to the positive areas cannot be excluded but evidence in its favor is weak.

Analogous experiments were done with the same or closely related polymer samples, but using different experimental arrangements. In one case, the HDPE film was sheared with a spinning PTFE stub. Electrostatic potential maps of the sheared film are in Fig. 4 and infrared spectra of spots in the negative area and in pristine HDPE are also in this Figure. The presence of peaks assigned to a C–F stretching vibration at 1230 and 1160 cm^{-1} show that fluorocarbon material was transferred to PTFE in the negative area; this was also described in the literature.[32] The positive area on PTFE film does not contain an amount of fluorocarbon detectable by this technique.

BEI and SEI micrographs of an HDPE film charged by shearing with a spinning PTFE stub are shown in Fig. 5, while elemental distribution maps are shown in Fig. 6. Mechanical damage on HDPE film is easily observed as well as the deposition of bits of fluorinated material, that appear as bright spots in the BEI micrographs. Fig. 5 and 6 show also some debris that are not fluorinated, as previously observed in the experiments done with PTFE film and LDPE foam.

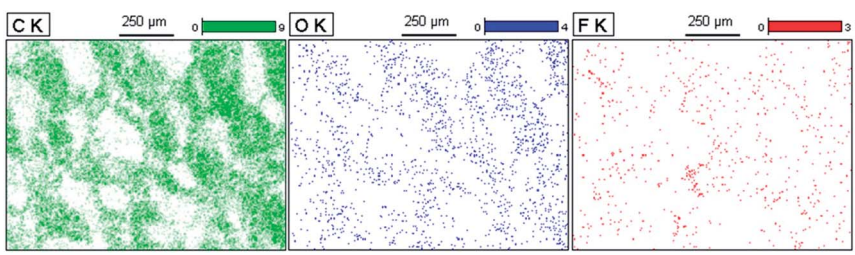

Fig. 3 EDX elemental distribution maps of a negative area of LDPE foam. Note the superposition of the dotted areas in the C, O and F maps and the variability of dot density.

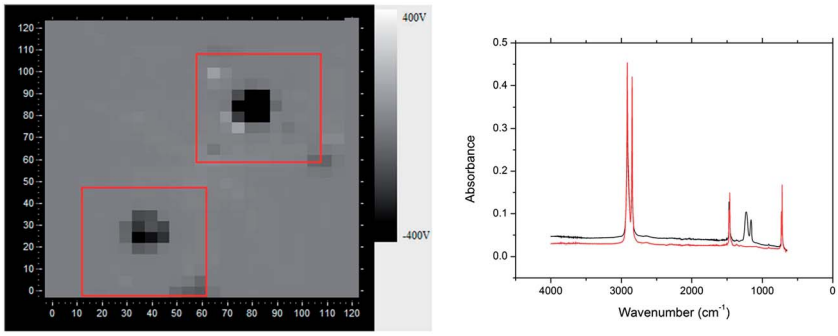

Fig. 4 (Left) Electrostatic potential maps of HDPE film sheared with a PTFE stub. (Right) Infrared spectra of a sheared area carrying negative charge (black) and a pristine area (red) of HDPE film tribocharged with PTFE.

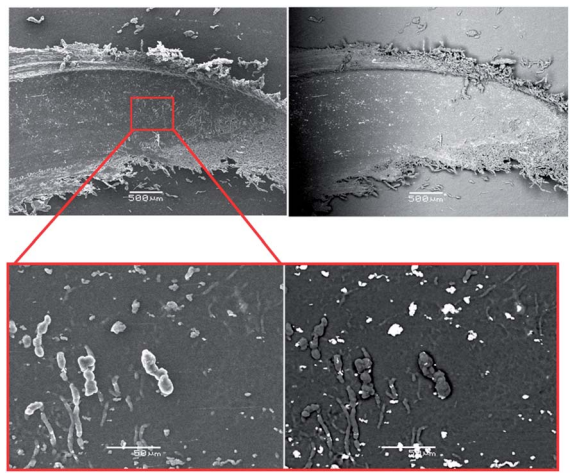

Fig. 5 SEI (left) and BEI (right) micrographs of an area of HDPE film sheared with a PTFE stub.

In other experiments, PTFE films were rubbed with HDPE stubs and they also acquired charge. The C : F atom ratio determined by EDX point analysis in the PTFE film was 1 : 0.65 instead of the expected 1 : 2 for PTFE, showing that PTFE coverage with HDPE fragments is partial.

A HDPE stub was imaged after rubbing PTFE film, SEI and BEI views are in Fig. 7, showing large debris laying on the stub surface. Microanalysis of this sample (Table 1) shows the presence of fluorine unevenly scattered in the debris surface, especially at the side which was likely formed during the tribocharging process. An intriguing feature of this sample is the presence of significant amounts of N in apparently undamaged spots of the stub surface, while O is found in all the six areas analysed. This may be understood by assuming that an atmospheric- or tribo-plasma[33] is formed in this system and its high-energy species react on the HDPE surface.

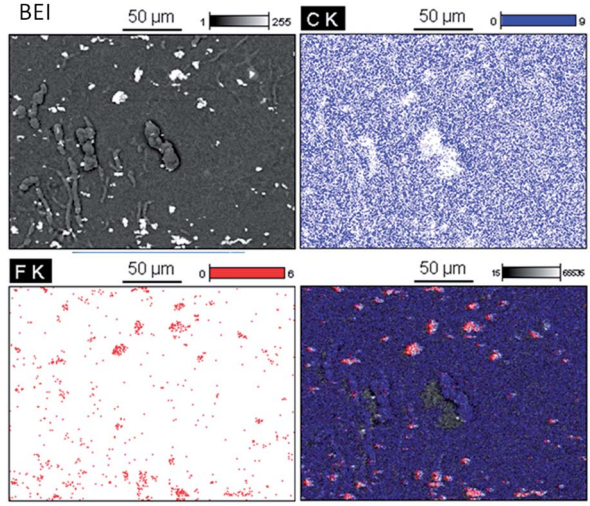

Fig. 6 Carbon and fluorine elemental distribution maps for the magnified area shown in Fig. 5. Note the correspondence between the bright spots in the BEI image and fluorine-rich areas in the elemental map.

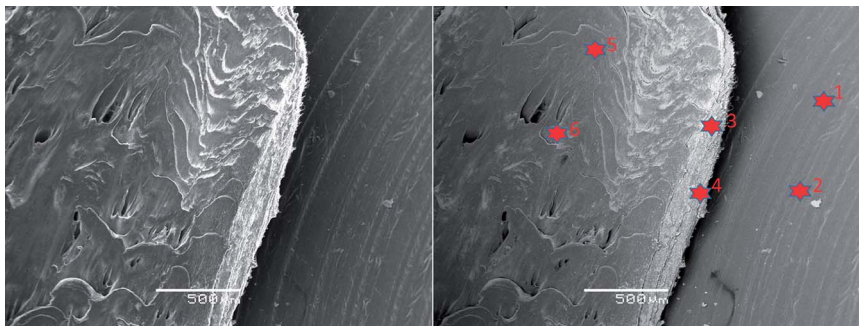

Fig. 7 (Left) SEI and (right) BEI micrograph of an area of a HDPE stub after rubbing PTFE film. The original stub surface is identified by the regular lines formed by the machining tool. Microanalysis data for the six points identified in the BEI micrograph are in the Table 1.

Table 1 Detected atom % determined by EDX point analysis in six spots of the area shown in Fig. 7

Spot	C (%)	N (%)	O (%)	F (%)
1	76.9	17.5	5.6	—
2	79.1	15.5	5.5	—
3	74.4	—	1.2	24.4
4	85.4	—	3.5	11.1
5	94.1	—	2.8	3.1
6	89.5	—	2.8	7.6

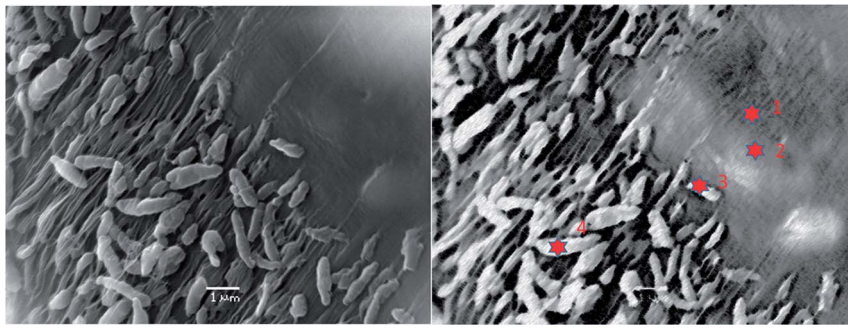

Fig. 8 SEI (left) and BEI (right) micrographs of a HDPE stub after rubbing PTFE film: left, SEI; right, BEI. The microanalysis data for the four points identified in the BEI micrograph are in Table 2.

Fig. 8 shows micrographs from another field of the surface of the HDPE stub shown in Fig. 7, with many interesting features concerning both the surface morphology and distribution of chemical constituents. First, the smooth surface in the first quadrant (upper right of the BEI image) shows flat contrasting domains with marked contrast between features as small as 100 nm and as large as 1 micron. Fractal dimensions were calculated for the flat areas in both images, yielding $D = 1.55 \pm 0.01$ for the SEI micrograph and 1.85 ± 0.02 for BEI and showing that chemical composition fluctuations follow a more complex pattern than the surface topography. Strained HDPE forming thin stripes connected to the flat matrix is also seen in the third quadrant (lower left) and adjacent areas. The surfaces of the seemingly particulate material are brighter than most other regions and they contain significant amounts of F, as shown in Table 2. This confirms that small domains containing PTFE fragments (and probably also other contaminants) are dispersed throughout this area.

A more comprehensive view of mass transfer and constituent distribution is obtained by elemental mapping at low magnification in an area of the HDPE stub that sheared PTFE, shown in Fig. 9. Fluorine-rich debris lies on top of the stub surface, while N and O are scattered unevenly throughout the surface.

Fig. 10 shows potential maps of films of PTFE and HDPE that were sheared with stubs made out of the same polymer: PTFE films sheared with PTFE stubs and HDPE films sheared with HDPE stubs. The formation of tribocharged domains is also observed but with some curious features. It is possible to observe the formation of positive domains on the PTFE film together with negative domains, even though this polymer usually tends to form anionic fragments only when rubbed with

Table 2 Detected atom % determined by EDX point analysis in spots of the area shown in Fig. 8

Spot	C	N	F
1	93.9	—	6.1
2	92.2	—	7.8
3	89.5	—	10.5
4	72.4	11.2	16.4

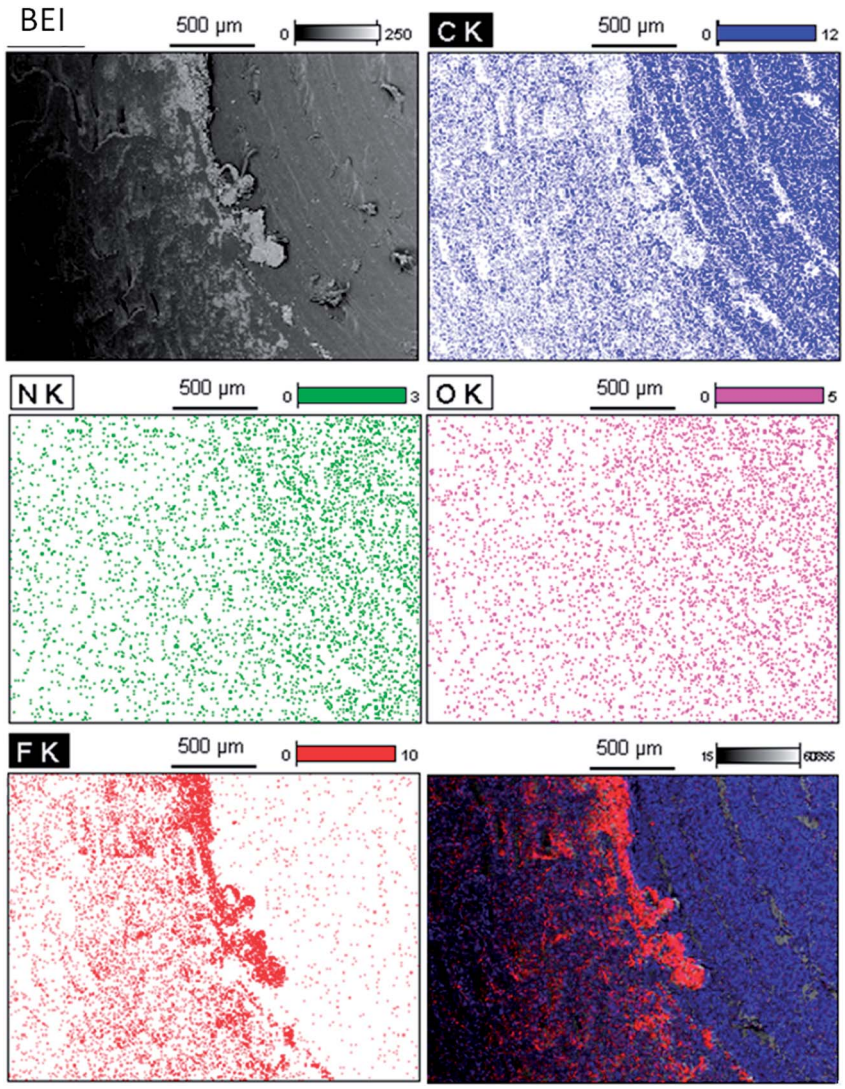

Fig. 9 Elemental maps of an area of the HDPE stub surface that sheared a PTFE film.

polyethylene. However, overall negative charge formation is observed in the stub, where a −200 V potential is measured. On the other hand, HDPE films are positively charged and the overall potential on the rubbing HDPE stub is low.

Maximum, minimum and mean square potential averages obtained for potential maps acquired in repeated independent runs are given in Fig. 10, showing the same pattern but with large quantitative differences. The average potential in the films is positive in both cases, the maximum potential is 150 V in the HDPE film and 640 V in PTFE, while minimum potentials are, respectively, 20 V and −1235 V.

The results presented so far in this report refer to PTFE and PE samples under low pressure and high speed friction but charge patterns have also been obtained

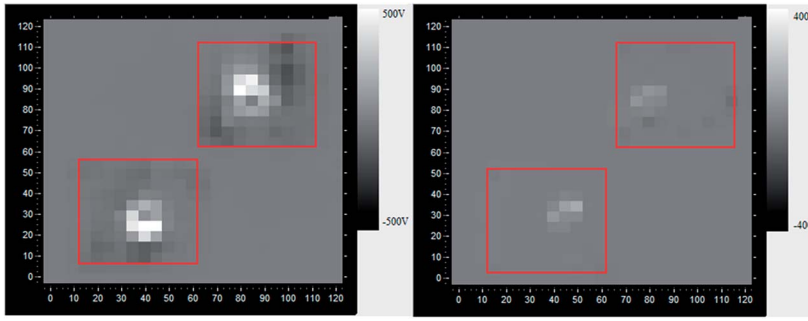

Fig. 10 (Left) Potential maps of PTFE films sheared with PTFE stubs and (right) of HDPE films sheared with HDPE stubs.

under other conditions. For instance, Fig. 11 shows micrographs of a PS slab sheared with PTFE stub, in a region where PTFE was detected. EDX point analysis on the bright fragments detects up to 20 atom percent F.

Electrostatic potential patterns have already been obtained for other polymer pairs. Pellets of different polyamides, HDPE and polyacetal were placed within PS Petri dishes and shaken in a reciprocating table, where the pellets undergo sliding motion. Table 3 shows the broad range of electrostatic potentials measured on a square in the central area of Petri dishes with the rubbing pellets. Data for HDPE film treated in the same way but with rolling PTFE spheres are also in this Table.

4 Discussion

The results described in this report confirm that the formation of charge by rubbing polymer surfaces is concurrent to mass transfer between the surfaces, without any exception among the systems examined so far. Spatial distribution of the transferred material is consistent with the formation of fractal charge patterns extending from the nano- to macroscopic scale, showing in most cases the coexistence of domains with positive and negative excess charge. Thus, the analytical electron micrographs and spectra presented here lead to a more complete explanation for the counter-intuitive charge segregation into separate

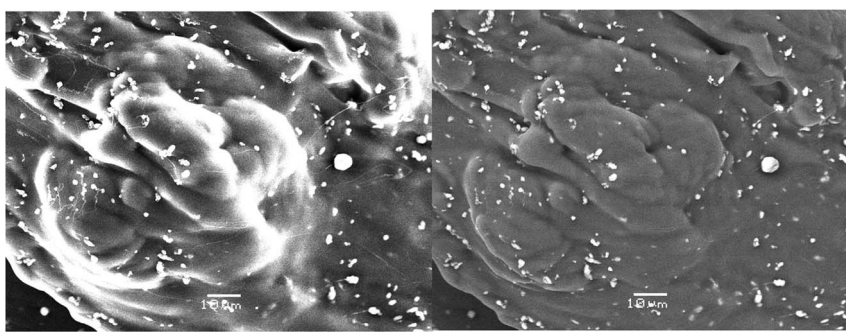

Fig. 11 Micrographs of a PS slab sheared with a PTFE stub. Left, SEI; right, BEI.

Table 3 Maximum, minimum and average potential of the central areas of PS Petri dishes shaken with polymer pellets and of a square HDPE film shaken with PTFE spheres. Pellets and spheres were not removed prior to potential measurements

Base surface	Moving pellets	Maximum potential/V	Minimum potential/V	Average potential/V	Standard deviation/V
Polystyrene (Petri dish)	Nylon 6	1185	−1780	160	685
	Nylon 6,9	830	−1010	45	390
	Nylon 12	770	−1170	−90	500
	HDPE	245	−705	−190	260
	Polyacetal	2231	2320	−657	1155
HDPE film	PTFE sphere	1550	−855	480	490

domains instead of the expected ion pairing that would contribute to abate the overall charge on the sample. On the other hand, this derives from the polymer structure and is different from findings made in other types of materials. Plastic deformation produced by indentation is the source of electric potential differences in pure and doped NaCl crystals[34] and it probably also plays a role in polymer friction, but the methods used in the present work do not allow an assessment of its relative importance.[35,36]

The backscattered-electron micrographs as well as the elemental maps agree in showing that lumps of one polymer material are pulled out and transferred to the other surface, carrying charge to it. Thus, they create large charge density fluctuations across the surface, making a strong contribution to the complex and irregular potential patterns that have been reported in recent work. On the other hand, the larger lumps shown in this work are not easily detected by other techniques such as Kelvin force microscopy (KFM), due their height which introduces significant imaging artefacts and also due to the amount of localized charge, which provokes strong deformation even on stiff KFM cantilevers.

The BEI and EDX micrographs frequently convey the same information, even though they are not expected to be always in full agreement, since the sampling depth is not the same in both cases (typically in the micron and sub-micron range). Moreover, they depend on the beam energy used in each imaging experiment and this is not kept constant, to increase the amount of information from each image. For this reason, a thin fluorine-rich surface layer may appear brighter in the BEI picture but point analysis may not show a large fluorine content, since the X-rays map a thicker surface layer.

There are two additional factors for charge patterning in polymer surfaces, beyond the formation of polymer ions. First, the charge on solid surfaces is exchanged with atmospheric or adsorbed water,[16,23,24] attracting OH^- and H^+ ions[37] to, respectively, the positive and negative surface sites. Incidentally, neat water surfaces are basic due to preferential adsorption of OH^- ions.[38] Also, the rapid formation and deposition of charged material on both rubbing surfaces should create large electrostatic potential fluctuations thus producing electric fields exceeding the thresholds for electrostatic discharge throughout the adjacent atmosphere. At this time, this is the best tentative explanation for the unexpected appearance of nitrogen bound to polymer surfaces that was detected in some samples.

Otherwise, the arguments for charge formation that were put forward earlier still prevail: charge formation is due to homolytic or heterolytic polymer chain breakdown under shearing. In the case of homolytic scission, electron transfer to and from neighbouring polymer free-radicals or molecules, as well as to atmospheric molecules and eventual polymer contaminants, leads to the formation of polymer ions.

Since chain breakdown is most likely at the surfaces of polymer particles pulled out of the surface during surface rubbing, a large fraction of the charges remain accumulated rather than dispersed throughout the tribocharged surface. Particle removal by washing surfaces with suitable liquids is usually a simple task and this explains why a large fraction of the tribocharge is easily removed from various polymer surfaces by simple immersion in both polar and apolar liquids.[39]

The fractal dimension obtained from linescans drawn on SEI micrographs in this paper agrees with previous results obtained by atomic force microscopy, as expected considering that both are determined mainly by surface topography. On the other hand, the fractal dimension for the chemical composition contrast in the BEI images (1.85) is significantly higher than figures previously obtained from Kelvin potential maps (1.64–1.72).[40] This is explained by considering the existence of a smoothing factor for potential gradients that is discharged across the surrounding atmosphere. This levels-out potential features that exceed the threshold for discharge but without transfer of the charge carrier polymer fragments.

The interdependence of friction and wear is well acknowledged in the literature, not only in polymer systems but also in metals.[41] Coefficients of friction and wear are parameters describing the state of contact of bodies and they are not constants of the contacting materials.[42,43] Wear and friction have been explained in terms of roughness, hardness, ductility, oxide film formation, reaction layers and transfer[42] but the formation of strongly charged tribolayers seems to be more conspicuous in polymers than in other types of materials. The recent recognition of the effect of tribocharges on friction coefficients[22] followed the work of nanotribologists[44–47] who paid due attention to the effect of surface charge on friction coefficients. This adds one more point to be considered in the sequence of events triggered by mutual mechanical action of contacting surfaces, from the mechanochemical reactions to the formation of triboelectricity, wear, adhesion and changes in the friction coefficients. On the other hand, it shows that tribometer and related experiments could benefit from concurrent electrostatic potential measurements that not often done.

One additional point that should be brought to this discussion is the time-temperature superposition as introduced by Williams, Landel and Ferry.[48] This implies that the mechanical behavior of two polymers mutually acting at high speed or high frequency resemble that of the same polymer but at some lower temperature, following a non-Arrhenius pattern. In practice, this means that polyethylene behavior at high frequency or high speeds resembles its behavior at a lower temperature, when the polymer is harder and less ductile. For this reason, simply contacting polymer surfaces or applying different types of mechanical action at different speeds should be expected to produce different chemical, structural, morphological and electrostatic results analogous to those described by Distler in ionic solids.[49]

To sum up, mechanochemical reactions triggered by friction produce ionic polymer chain fragments, especially at the surface of particles pulled away from the rubbing surfaces that can be transferred from one rubbing body surface to another. Amphiphilic species are thus formed, containing charged end-groups that are excluded from the polymer–air interface, since their contribution to the material surface tension is more positive than the contribution of other, less polar groups. Charges are thus occluded and partly protected from water adsorbed at the polymer surface and from water vapor or aerosols, explaining the tribocharge stability that was previously reported.

5 Conclusion

Tribolayer formation in polymers is initiated by mechanochemical reactions during friction producing free-radicals that are at least partly transformed into ionic species with half-lives exceeding tens of hours and have a major if not dominating role in the formation of triboelectricity. This explains the ubiquity of charge patterns on insulating polymer surfaces following contact with any other materials, which has been evidenced for the past fifteen years, including patterns obtained by rubbing two identical solids. Moreover, it supports a new explanation for the dissipative character of friction, based on the large enthalpy requirements for the scission of strong carbon–carbon covalent bonds.

Acknowledgements

This is a contribution from the INCT Inomat, a project supported by Brazilian agencies MCTI/CNPq and Fapesp. L. B. S. B. and D. D. D. acknowledge graduate fellowships from Fapesp and CNPq.

References

1 G. S. P. Castle and L. B. Schein, *J. Electrost.*, 1995, **36**, 165.
2 L. B. Schein, *Science*, 2007, **316**, 1572.
3 A. G. Bailey, *J. Electrost.*, 2001, **51–52**, 82.
4 M. W. Williams, *IEEE Trans. Ind. Appl.*, 2011, **47**, 1093.
5 M. W. Williams, *Am. Sci.*, 2012, **100**, 316.
6 M. W. Williams, *AIP Adv.*, 2012, **2**, 010701.
7 D. J. Lacks and R. M. Sankaran, *J. Phys. D: Appl. Phys.*, 2011, **44**, 453001.
8 M. Glor, *J. Electrost.*, 1985, **16**, 175.
9 N. Gibson, *J. Electrost.*, 1997, **40–41**, 21.
10 L. Perrin, A. Laurent, V. Falk, O. Dufaud and M. Traoré, *J. Loss Prev. Process Ind.*, 2007, **20**, 207.
11 A. Galembeck, C. A. R. Costa, M. C. V. M. da Silva, E. F. Souza and F. Galembeck, *Polymer*, 2001, **42**, 4845.
12 E. Teixeira Neto and F. Galembeck, *Colloids Surf., A*, 2002, **207**, 147.
13 A. L. H. Cardoso, C. A. P. Leite and F. Galembeck, *Langmuir*, 1999, **15**, 4447.
14 H. T. Baytekin, A. Z. Patashinski, M. Branicki, B. Baytekin, S. Soh and B. A. Grzybowski, *Science*, 2011, **333**, 308.
15 Y. Martin, C. C. Williams and H. K. Wickramasinghe, *J. Appl. Phys.*, 1987, **61**, 4723.

16 C. A. Rezende, R. F. Gouveia, M. A. da Silva and F. Galembeck, *J. Phys.: Condens. Matter*, 2009, **21**, 263002.
17 T. A. L. Burgo, T. R. D. Ducati, K. R. Francisco, K. J. Clinckspoor, F. Galembeck and S. Galembeck, *Langmuir*, 2012, **28**, 7407.
18 R. P. Feynman, R. B. Leighton and M. Sands, *The Feynman Lectures on Physics*, 1, 2nd edn, Addison-Wesley Publishing Company, Reading MA, 2005, pp. 4–7.
19 A. F. Diaz and R. M. Felix-Navarro, *J. Electrost.*, 2004, **62**, 277.
20 P. J. Flory, *J. Chem. Phys.*, 1942, **10**, 51.
21 M. J. Huggins, *The Journal of Physical Chemistry*, 1942, **46**, 151.
22 T. A. L. Burgo, C. S. Souza, L. B. S. Balestrin and F. Galembeck, *Sci. Rep.*, 2013, **3**, 2384.
23 R. F. Gouveia and F. Galembeck, *J. Am. Chem. Soc.*, 2009, **131**, 11381.
24 J. S. Bernardes, C. A. Rezende and F. Galembeck, *J. Phys. Chem. C*, 2010, **114**, 19016.
25 H. T. Baytekin, B. Baytekin, T. M. Hermans, B. Kowalczyk and B. A. Grzybowski, *Science*, 2013, **341**, 1368.
26 C. M. Pooley and D. Tabor, *Proc. R. Soc. London, Ser. A*, 1972, **329**, 251.
27 V. Quaglini and P. Dubini, *Adv. Tribol.*, 2011, 178943.
28 J. Ye, H. S. Khare and D. L. Burris, *Wear*, 2013, **297**, 1095.
29 T. A. Blanchet and F. E. Kennedy, *Wear*, 1992, **153**, 229.
30 C. Lhymn, *Wear*, 1986, **107**, 95.
31 D. W. Breiby, T. I. Sølling, O. Bunk, R. B. Nyberg, K. Norrman and M. M. Nielsen, *Macromolecules*, 2005, **38**, 2383.
32 A. I. Sviridyonok, V. A. Bely, V. A. Smurugov and V. G. Savkin, *Wear*, 1973, **25**, 301.
33 G. Heinicke, *Tribochemistry*, Hanser, Munich, 1984.
34 F. Frohlich and P. Seifert, *Phys. Status Solidi B*, 1968, **25**, 303.
35 W. M. Rainforth, P. Zeng, L. Ma, A. N. Valdez and T. Stewart, *Faraday Discuss.*, 2012, **156**, 41.
36 A. Vernes, S. Eder, G. Vorlaufer and G. Betz, *Faraday Discuss.*, 2012, **156**, 173.
37 L. P. Santos, T. R. D. Ducati, L. S. Balestrin and F. Galembeck, *J. Phys. Chem. C*, 2011, **115**, 11226.
38 J. K. Beattie, A. N. Djerdjev and G. G. Warr, *Faraday Discuss.*, 2009, **141**, 31.
39 K. R. Francisco, T. A. L. Burgo and F. Galembeck, *Chem. Lett.*, 2012, **41**, 1256.
40 J. P. Santos, P. Corpart, K. Wong and F. Galembeck, *Langmuir*, 2004, **20**, 10576.
41 F. P. Bowden and D. Tabor, *The Friction and Lubrication of Solids*, Oxford, Clarendon, 2001, p. 341.
42 K. Kato, *Wear*, 2000, **241**, 151.
43 T. Polcar, F. Gustavsson, T. Thersleff, S. Jacobson and A. Cavaleiro, *Faraday Discuss.*, 2012, **156**, 383.
44 C. M. Mate, G. M. MacClelland, R. Erlandsson and S. Chiang, *Phys. Rev. Lett.*, 1987, **59**, 1942.
45 D. F. Ogletree, R. W. Carpick and M. Salmeron, *Rev. Sci. Instrum.*, 1996, **67**, 3298.
46 G. Marti and N. D. Spencer, *Langmuir*, 1995, **11**, 4632.
47 R. W. Carpick, N. Agrait, D. F. Ogletree and M. Salmeron, *Langmuir*, 1996, **12**, 3334.
48 M. L. Williams, R. F. Landel and D. Ferry, *J. Am. Chem. Soc.*, 1955, **77**, 3701.
49 G. I. Distler, *Krist. Tech.*, 1970, **5**, 73.